JOURNAL OF THERMOPHYSICS AND HEAT TRANSFER
Vol. 25, No. 2, April–June 2011

Numerical Analysis of Heated Channel Flows by a Space-Marching Finite Volume Technique

Annafederica Urbano* and Francesco Nasuti†
University of Rome "La Sapienza," 00184 Rome, Italy

DOI: 10.2514/1.51741

The design phase of devices involving many different flow phenomena requires efficient numerical simulations that, although based on some approximations, are able to manage complex flow modeling and fluid–structure interaction. The attention of the present study is devoted to liquid rocket engine cooling-channel flows, whose main characteristics to be taken into account are high wall heat flux, of the order of 10 MW/m^2; high flow Reynolds number, of the order of 10^6–10^7; fully-three-dimensional flow; near-critical thermodynamic conditions of the fluid; fluid decomposition reactions; and coupling between flow and wall temperature evolution. The proposed approximation is to use parabolized Navier–Stokes equations. Parabolization is obtained by neglecting viscous derivatives in the space-marching direction and by considering the streamwise pressure gradient as a source term evaluated on the basis of the overall momentum balance. The algorithm is based on a finite volume approach, which uses a modified Roe's approximate Riemann solver for a fluid governed by a generic equation of state. Validation of the approach is presented by comparison of the channel-flow results with full Navier–Stokes solutions and experimental data. Results show that the present approach is a practicable one for the study of cooling properties of real fluids in channels.

Nomenclature

$\mathcal{A}_{x,i}$	=	area of the cell-face surface perpendicular to the longitudinal direction
c_p	=	specific heat at constant pressure
D	=	diameter of the channel cross section
d	=	distance from the closest wall
$\mathbf{F}_e$	=	vector of Eulerian fluxes in the streamwise direction
$\bar{\mathbf{F}}_e$	=	parabolized vector of Eulerian fluxes in the streamwise direction
$\mathbf{G}_e$, $\mathbf{H}_e$	=	vectors of Eulerian fluxes in the transverse directions
$\mathbf{G}_v$, $\mathbf{H}_v$	=	vectors of viscous fluxes in the transverse directions
H	=	height of the channel cross section
h	=	enthalpy
h_0	=	total enthalpy
k	=	thermal conductivity
L	=	channel length
M	=	Mach number
n	=	direction normal to the longitudinal lateral surface
$\mathbf{P}$	=	pressure term vector for parabolized Navier–Stokes equations
Pr	=	Prandtl number
p	=	pressure
$\mathbf{Q}$	=	source-term vector
q	=	heat flux
$\mathcal{S}$	=	surface
S	=	vorticity module
$\tilde{S}$	=	corrected vorticity module
$\mathcal{S}_{c,i}$	=	surface of the channel cross sections at x_i
$\mathcal{S}_{l,i}$	=	cell-face surface parallel to the longitudinal direction between the integration abscissas x_i and x_{i+1}
$\mathcal{S}_{w,i}$	=	channel-wall surface spanning between the cross sections at x_i and x_{i+1}
$\mathcal{S}_{x,i}$	=	cell-face surface perpendicular to the longitudinal direction
T	=	temperature
u	=	streamwise velocity component
v, w	=	transverse velocity components
x	=	streamwise direction and coordinate
y, z	=	transverse directions and coordinates
y^+	=	nondimensional wall distance
μ	=	viscosity
$\tilde{\mu}$	=	integration variable of the turbulence-model equation
$\tilde{\nu}$	=	corrected kinematic turbulent viscosity used in the turbulence-model equation
ρ	=	density
τ	=	wall shear stress
Ω	=	vorticity vector components
ω	=	Vigneron parameter

Subscripts

b	=	bulk
c	=	critical value
i	=	cell index in the streamwise direction x
in	=	inlet
j	=	cell index in the transverse direction y
k	=	cell index in the transverse direction z
t	=	turbulent viscosity, conductivity, and Prandtl number
w	=	wall
1,. . .,5	=	first–fifth components of flux vectors
6	=	turbulence-model equation component of flux vectors (sixth component)

Presented as Paper 2010-4315 at the 10th AIAA/ASME Joint Thermophysics and Heat Transfer Conference, Chicago, IL, 28 June–1 July 2010; received 27 July 2010; revision received 9 November 2010; accepted for publication 9 November 2010.

*Ph.D. Student, Dipartimento di Ingegneria Meccanica e Aerospaziale, Via Eudossiana 18. Student Member AIAA.

†Associate Professor, Dipartimento di Ingegneria Meccanica e Aerospaziale, Via Eudossiana 18. Senior Member AIAA.

I. Introduction

COOLING of liquid rocket engine thrust chambers is a mandatory task because of the high temperature reached by the burned propellant gas. Among the possible choices for the cooling system, regenerative cooling is often selected because of its good efficiency. In this case, the fluid flows in channels surrounding the thrust chamber; as a consequence, the study of flow evolution in these channels is necessary for both thrust-chamber thermal design and system analysis, especially in the case of closed-cycle

turbopump-fed engines. The numerical study of flow evolution in the channels is a necessary tool for the design of future engines, as demonstrated from the many studies on the subject [1–9]. However, to understand the difficulties of getting a reliable numerical simulation, the following aspects have to be considered: channels are long and narrow; the flow inside channels is strongly three-dimensional; wall temperature, hot-gas flow evolution, and coolant flow evolution are strongly coupled with each other; coolant can be either liquid or gas or supercritical fluid or in near-critical thermodynamic conditions; flow Reynolds number can be of the order of $10^6 \div 10^7$; wall heat flux can be of the order of 10 $\mathrm{MW/m^2}$; and fluid decomposition reactions can occur [10]. If all of these aspects have to be taken into account, it can be inferred that solving the full unsteady Navier–Stokes equations can still be cumbersome in the design phase. In fact, simplified one-dimensional or quasi-two-dimensional approaches, which strongly rely on empirical correlations, are still in use [2,4,11].

In this context, the aim of the present study is to develop a simplified approach based on the solution of parabolized Navier–Stokes (PNS) equations. This reduced set of equations falls between the full Navier–Stokes (FNS) equations and the boundary-layer equations in terms of complexity. Three groups of simplified Navier–Stokes equations have been defined in the literature and have been used to study viscous supersonic external flows: parabolized Navier–stokes equations; thin-layer Navier–Stokes equations; and reduced Navier–Stokes equations [12–14]. Channel flows have also been studied with simplified Navier–Stokes equations, which belong to the family of PNS [15–17]. Partially parabolized Navier–Stokes equations [18,19], for which a multiple-sweep marching method is required, have also been considered for the study of the channel flows. An exhaustive review of the different numerical approaches used to solve simplified Navier–Stokes equations is presented in [12,20]. All of these different numerical strategies share the common characteristic that the steady form of the governing equations is employed, and the solution is "marched" in space, so that a typical problem is reduced from four to three dimensions. In a channel, this approach allows one to solve the equations by marching in space in the main flow direction. In general, this could be done only if the flow is supersonic. On the contrary, in the present channel flows the whole flow is subsonic. Therefore, some assumptions have to be made to treat the backward-propagating signals: the strategy for treating the pressure gradient in the streamwise direction is one of the main differences between the different PNS schemes known in the literature.

Although solutions in the field of the cooling channels with similar approaches have been presented in the literature [1], the final aim of the present work is to study the whole regenerative cooling system of a liquid rocket engine with a low computational cost, including the main thermodynamic and fluid–structure interaction phenomena. The present study follows the approach of a single streamwise sweep; the pressure gradient in the space-marching direction is treated as a source term that is evaluated by considering the overall conservation of the momentum equation. Both laminar and turbulent flows have been studied with the present approach for real fluids described by a generic equation of state. Validation has been carried out for 2-D planar and axisymmetric test cases by comparison with results obtained by a validated full Navier–Stokes solver [5]. Moreover, comparisons with full Navier–Stokes solutions and experimental data are provided for a near-critical hydrogen test case [7,21]. This test case is of particular interest because it presents heat transfer deterioration, which is a phenomenon that can occur with near-critical fluids for high heat fluxes and is difficult to reproduce numerically.

II. Governing Equations

The parabolization of Navier–Stokes equations is obtained by considering that a channel flow has a predominant flow direction. On this basis, the following assumptions can be made:

1) The derivatives in the streamwise direction in the diffusive terms are of lower order of magnitude than the same derivatives in the transverse directions.

2) The velocity in the streamwise direction is always positive; no reverse flow occurs.

3) The pressure gradient in the streamwise direction is constant along each transverse plane.

Under these assumptions a fully parabolized form of the steady Navier–Stokes equations can be considered to describe the flow behavior. Considering a Cartesian reference system for a straight tube, if x is the streamwise direction and y and z are the transverse directions, then the conservative form of the three-dimensional PNS equations is

$$\frac{\partial \mathbf{F}_e}{\partial x} + \frac{\partial \mathbf{G}_e}{\partial y} - \frac{\partial \mathbf{G}_v}{\partial y} + \frac{\partial \mathbf{H}_e}{\partial z} - \frac{\partial \mathbf{H}_v}{\partial z} = \mathbf{Q}\varpi\vartheta \tag{1}$$

where the subscripts e and v indicate the Eulerian and viscous flux vectors, respectively, after the PNS approximations have been applied. These equations have been obtained by neglecting the streamwise viscous flux vector and the x derivatives in the transverse viscous flux vectors (in $\mathbf{G}_v$ and $\mathbf{H}_v$, all the x derivatives have been neglected). A source-term vector $\mathbf{Q}$ has been emphasized in Eq. (1) for the sake of generality. The resulting expressions of the flux vectors are

$$\mathbf{F}_e = \begin{Bmatrix} \rho u \\ \rho u^2 + p \\ \rho uv \\ \rho uw \\ \rho u h_0 \end{Bmatrix} \qquad \mathbf{G}_e = \begin{Bmatrix} \rho v \\ \rho uv \\ \rho v^2 + p \\ \rho vw \\ \rho v h_0 \end{Bmatrix}$$

$$\mathbf{H}_e = \begin{Bmatrix} \rho w \\ \rho uw \\ \rho vw \\ \rho w^2 + p \\ \rho w h_0 \end{Bmatrix} \tag{2}$$

$$\mathbf{G}_v = \begin{Bmatrix} 0 \\ \mu \dfrac{\partial u}{\partial y} \\ \dfrac{3}{2}\mu\left(2\dfrac{\partial v}{\partial y} - \dfrac{\partial w}{\partial z}\right) \\ \mu\left(\dfrac{\partial v}{\partial z} + \dfrac{\partial w}{\partial y}\right) \\ uG_{v,2} + vG_{v,3} + wG_{v,4} + k\dfrac{\partial T}{\partial y} \end{Bmatrix} \qquad \mathbf{H}_v = \begin{Bmatrix} 0 \\ \mu \dfrac{\partial u}{\partial z} \\ \mu\left(\dfrac{\partial v}{\partial z} + \dfrac{\partial w}{\partial y}\right) \\ \dfrac{3}{2}\mu\left(2\dfrac{\partial w}{\partial z} - \dfrac{\partial v}{\partial y}\right) \\ uH_{v,2} + vH_{v,3} + wH_{v,4} + k\dfrac{\partial T}{\partial z} \end{Bmatrix} \tag{3}$$

where subscripts 2, 3, and 4 indicate, respectively, the second, third, and fourth components of vectors. The system of equations (1) is a parabolic system only if the flow is supersonic in the streamwise direction, whereas the pressure gradient in the x direction permits information to be propagated upstream in the case of subsonic flow. In the latter case, from a mathematical point of view, the system is elliptic. The influence of the streamwise pressure-gradient term on the mathematical nature of the PNS equations has been studied by Vigneron et al. [22], who showed that if only a fraction ω ($0 \le \omega \le 1$) of the streamwise pressure gradient ($\mathrm{d}p/\mathrm{d}x$) is retained

in the equations, the system also becomes parabolic in the case of subsonic flow. The value of the parameter ω that makes the system parabolic depends on the local flow Mach number. Nevertheless, the system is always parabolic if ω is set to 0: that is, if the streamwise pressure gradient is no longer considered as an unknown. In this case, the equation system is recasted as

$$\frac{\partial \bar{\mathbf{F}}_e}{\partial x}+\frac{\partial \mathbf{G}_e}{\partial y}-\frac{\partial \mathbf{G}_v}{\partial y}+\frac{\partial \mathbf{H}_e}{\partial z}-\frac{\partial \mathbf{H}_v}{\partial z}=\frac{\partial \mathbf{P}}{\partial x}+\mathbf{Q} \tag{4}$$

where the pressure gradient has been moved to the right-hand side to emphasize that it is considered as a source term of the parabolic system. The new symbols introduced with respect to Eq. (1) are

$$\bar{\mathbf{F}}_e=\begin{Bmatrix}\rho u\\ \rho u^2\\ \rho uv\\ \rho uw\\ \rho uh_0\end{Bmatrix} \qquad \mathbf{P}=\begin{Bmatrix}0\\ -p\\ 0\\ 0\\ 0\end{Bmatrix} \tag{5}$$

The streamwise pressure gradient is considered as a source term $\mathbf{P}$, which is either known a priori or evaluated on the basis of integral balance over the cross section, as will be discussed in the following.

III. Turbulence Model

Because of the high Reynolds number (of the order of 10^6), the flow in the channels of interest is turbulent. In the present study, the Reynolds-averaged Navier–Stokes approach is considered with a one-equation turbulence model. In particular, the convection–diffusion equation of Spalart and Allmaras [23] for the turbulent viscosity is included in the system (4) after the PNS hypothesis have been applied. Having neglected all the time and streamwise derivatives, the scalar Spalart–Allmaras equation can be written as

$$\frac{\partial F_{e,6}}{\partial x}+\frac{\partial G_{e,6}}{\partial y}-\frac{\partial G_{v,6}}{\partial y}+\frac{\partial H_{e,6}}{\partial z}-\frac{\partial H_{v,6}}{\partial z}=\frac{\partial P_6}{\partial x}+Q_6 \tag{6}$$

where the subscript 6 denotes the corresponding sixth component of flux and source vectors of Eq. (4). In Eq. (6) the convection (Eulerian) terms are

$$F_{e,6}=u\tilde{\mu} \qquad G_{e,6}=v\tilde{\mu} \qquad H_{e,6}=w\tilde{\mu} \tag{7}$$

and the diffusion (viscous) terms are

$$G_{v,6}=\frac{1}{\sigma}(\mu+\tilde{\mu})\frac{\partial \tilde{\nu}}{\partial y} \qquad H_{v,6}=\frac{1}{\sigma}(\mu+\tilde{\mu})\frac{\partial \tilde{\nu}}{\partial z} \tag{8}$$

where $\sigma=2/3$ and $\tilde{\nu}$ is related to $\tilde{\mu}$ through the relationship

$$\tilde{\mu}=\rho\tilde{\nu} \tag{9}$$

The pressure term is null ($P_6=0$). Finally, the first five components of the source term vector also continue to be null in the case of turbulent flows, and its sixth component, Q_6 in Eq. (6) is

$$Q_6=P_{\text{prod}}-P_{\text{dest}}+P_{\text{diff}} \tag{10}$$

where the production term is $P_{\text{prod}}=c_{b1}\tilde{S}\,\tilde{\mu}$, the destruction term is $P_{\text{dest}}=(c_{w1}f_w/\rho)(\tilde{\mu}/d)^2$, and the diffusion term is

$$P_{\text{diff}}=\frac{\rho c_{b2}}{\sigma}\left[\left(\frac{\partial \tilde{\nu}}{\partial y}\right)^2+\left(\frac{\partial \tilde{\nu}}{\partial z}\right)^2\right]$$

.

In the evaluation of the diffusion term, the difference with respect to the standard model is that streamwise derivatives are neglected. In the evaluation of the production and destruction terms, the values of the calibration constants c_{b1}, c_{w1}, c_{b2}, and σ are taken from [23], and f_w is an empirical function. The corrected vorticity module $\tilde{S}$ is also computed according to [23], except that the vorticity module $S=\sqrt{\Omega_x^2+\Omega_y^2+\Omega_z^2}$ is computed by neglecting the streamwise velocity derivatives. The components of the vorticity vector are therefore

$$\Omega_x=\frac{\partial v}{\partial z}-\frac{\partial w}{\partial y} \qquad \Omega_y=-\frac{\partial u}{\partial z} \qquad \Omega_z=\frac{\partial u}{\partial y} \tag{11}$$

The turbulence-model equation provides the value of the eddy viscosity through the relationship

$$\mu_t=\tilde{\mu}f_{v1} \tag{12}$$

between the eddy viscosity and the integration variable $\tilde{\mu}$. The empirical function f_{v1} is computed according to [23]. The value of μ_t computed in Eq. (12) has to be added to the molecular viscosity in Eq. (3). For the evaluation of the heat flux term in Eq. (3), the value of conductivity has to include a turbulent contribution k_t, which is evaluated on the basis of μ_t and a turbulent Prandtl number as follows:

$$k_t=\mu_t c_p/Pr_t \tag{13}$$

IV. Numerical Model

The numerical solution of Eq. (4), in which the streamwise pressure gradient is treated as a source term, is carried out by considering that the system of equations is parabolic in the streamwise direction and elliptic in the transverse directions: the equations can therefore be solved using a space-marching method. The present space-marching method relies on a finite volume scheme, in which the unknown $\bar{\mathbf{F}}_e$ fluxes are integrated in the x direction with an Euler explicit scheme once the $\mathbf{G}_e$, $\mathbf{G}_v$, $\mathbf{H}_e$, and $\mathbf{H}_v$ fluxes have been evaluated at the cell interfaces. Following this approach, and referring to the generic integration cell (i, j, k) of Fig. 1, Eq. (4) can be written as

$$\bar{F}_{e,i+1}=\bar{F}_{e,i}-\frac{1}{\mathcal{A}_{x,i}}\int_{\mathcal{S}_{l,i}}(\mathbf{G}_e n_y-\mathbf{G}_v n_y+\mathbf{H}_e n_z-\mathbf{H}_v n_z)\,\mathrm{d}\mathcal{S}+Q\Delta x+\Delta P \tag{14}$$

where $\Delta x=x_{i+1}-x_i$, $\Delta P=P_{i+1}-P_i$, and n_y and n_z are the components in the y and z directions, respectively, of the outward unit vector normal to the longitudinal surface of the integration cell. The $\bar{F}_{e,i}$ fluxes are considered constant over the single transverse cell-face surface of area $\mathcal{A}_{x,i}$, which provides the first order of the scheme. The viscous fluxes $\mathbf{G}_v$ and $\mathbf{H}_v$ are computed with central differences, whereas the Eulerian fluxes $\mathbf{G}_e$ and $\mathbf{H}_e$ at each cell interface are obtained as the solutions of a Riemann problem. The Riemann solver is a modified version of the Roe's approximate Riemann solver [24] for Eq. (4) with generic equations of state:

$$h=h(p,\rho) \qquad T=T(p,\rho)\cdots \tag{15}$$

where h is enthalpy, T is temperature, p is pressure, and ρ is density. Once all the eigenvalues have been evaluated, a Courant–Friedrichs–Lewy condition permits choosing a Δx integration step that provides

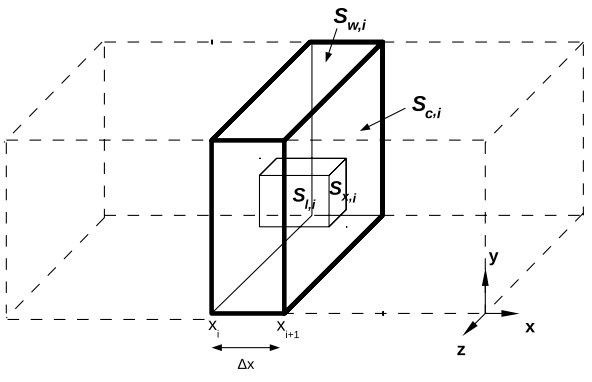

Fig. 1 Schematic of a generic 3-D control volume.

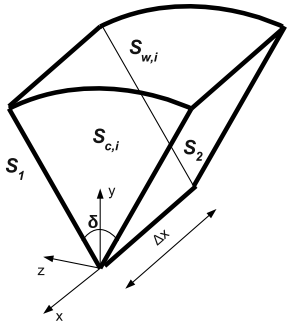

Fig. 2 Schematic of a 2-D axisymmetric integration domain.

a stable scheme. The equations of state (15) and transport properties are computed according to [25,26] and discretized in a database; during the solving process, the properties are taken from the database that also includes the necessary thermodynamic derivatives [5].

A. Streamwise Pressure Gradient

One of the critical points of the algorithm is how to compute the streamwise pressure gradient, which has to be evaluated at each integration step. The **P** term in Eq. (4) is evaluated with an iteration process, imposing the conservation of the integral momentum equation for each step of the channel of length Δx. Referring to Fig. 1, the pressure variation has to verify the following balance equation:

$$\int_{\mathcal{S}_{c,i+1}} (\rho u^2 + p)\,\mathrm{d}S = \int_{\mathcal{S}_{c,i}} (\rho u^2 + p)\,\mathrm{d}S - \int_{\mathcal{S}_{w,i}} \mu \frac{\partial u}{\partial n}\,\mathrm{d}\mathcal{S} \quad (16)$$

where $\mathcal{S}_{c,i+1}$ indicates the surface of the channel cross section, and $\mathcal{S}_{w,i}$ is the wall surface of the channel in the length Δx. For example, for a 2-D planar channel, Eq. (16) becomes

$$\frac{\mathrm{d}}{\mathrm{d}x}\left(\int_0^H (\rho u^2 + p)\,\mathrm{d}y\right) - \left(\mu \left.\frac{\partial u}{\partial y}\right|_H - \mu \left.\frac{\partial u}{\partial y}\right|_0\right) = 0 \quad (17)$$

where H is the height of the channel. It is assumed that the pressure gradient in the streamwise direction does not depend on the transverse position in the transverse plane.

B. Two-Dimensional Axisymmetric

In the finite volume approach the 2-D axisymmetric case is obtained with a suitable control volume and suitable boundary conditions. The 2-D axisymmetric integration domain used in the present simulations is a cylinder slice, as shown in Fig. 2. A symmetry boundary condition is imposed on the lateral surfaces S_1 and S_2, and a viscous wall boundary condition is imposed on the channel surface $S_{w,i}$. The symmetry axis (x axis in Fig. 2) is a degenerate surface, where all the fluxes are assumed to be zero.

V. Validation: Comparison Between PNS and FNS Results

To validate the PNS solver for a perfect gas, either in a laminar or turbulent condition, comparisons have been made with the results obtained with the full Navier–Stokes solver presented in [5] for a 2-D planar flow and a 2-D axisymmetric flow. The fluid is air in a perfect-gas condition. The parameters of all the test cases presented in the following are listed in Table 1.

A. Two-Dimensional Planar Flow

Results obtained with the FNS and PNS solvers for 2-D planar channels are compared for the following two test cases: laminar adiabatic flow in test case 1 (TC1) and turbulent nonadiabatic flow in test case 2 (TC2).

Inlet and outlet boundary conditions have to be imposed in the full Navier–Stokes code: the stagnation state at the entrance (pressure and temperature) and the static exit pressure. The geometric parameters of the computational domain (L is the length of the channel) are reported in Table 1. The density, pressure, and velocity profiles at a distance $L/2$ from the entrance ($x = 0$) are enforced as the initial condition of the PNS simulations; the results are compared in the remaining $L/2$ length of the channel. Pressure, temperature, and Mach number at the entrance of the channel of the PNS simulations are also reported in Table 1. The bulk pressure and the wall shear stress obtained with the two codes are compared in the Fig. 3 for the laminar test case. The displacement of the PNS solution with respect to the FNS solution is quite small; the maximum discrepancy is 0.15% on the bulk pressure and 0.5% on the wall shear stress. For the turbulent heated-flow test case TC2 (Fig. 4), the comparison on the wall temperature T_w is displayed instead of the wall shear stress. As can be seen in this case, the discrepancies are very small; the biggest discrepancy is on the wall temperature with a difference of 1% (Fig. 4b). These differences are as large, as expected, because of the PNS approximation.

B. Two-Dimensional Axisymmetric Flow

As for the 2-D planar test cases, the 2-D axisymmetric flow validation comparisons have been made between the results obtained with the FNS and the PNS codes. The following test cases are analyzed: laminar nonadiabatic flow (TC3) and turbulent adiabatic and nonadiabatic flows (TC4, TC5, and TC6).

Figure 5 illustrates the comparisons for the bulk pressure and the wall temperature for the laminar test case; it is a nonadiabatic flow with constant heat load along the channel $q_w = 10^4$ W/m^2 (TC3 of Table 1). As can be seen, the discrepancies are as small as in the 2-D planar cases; the biggest discrepancy is on the wall temperature, with a difference of 0.5%. The comparisons for the turbulent test cases are presented in Figs. 6–8; TC4 is an adiabatic test case, and TC5 and TC6 are heated flows with a constant heat load along the channel of $q_w = 10^4$ and 10^5 W/m^2, respectively. The analysis of these solutions shows a very good agreement for the bulk pressure, with discrepancies smaller than 0.05%. The differences on the wall shear stress and temperature are smaller than 5%, and the trends of the PNS and FNS results are the same.

VI. Validation: Comparison with Experimental Data

The good agreement between the results obtained with the PNS and the FNS solvers demonstrates that the terms neglected because of the PNS hypothesis are of minor importance in channel test cases. However, to extend the analysis to other possible situations occurring inside rocket engine cooling channels, the case of heating of a supercritical-pressure/subcritical-temperature fluid has been considered as a further validation test. Moreover, a longer channel than

Table 1 Test-case inlet conditions and geometric parameters

Test case	Fluid	Geometry	Flow	p_{in}, MPa	T_{in}, K	M_{in}	q_w, MW/m^2	D or H, mm	L, cm
TC1	Air	Planar	Laminar	0.164	424	0.60	0.00	5	100
TC2	Air	Planar	Turbulent	0.234	412	0.21	0.10	5	25
TC3	Air	Axisymmetric	Laminar	0.243	311	0.14	0.01	4	50
TC4	Air	Axisymmetric	Turbulent	0.244	304	0.12	0.00	4	10
TC5	Air	Axisymmetric	Turbulent	0.244	312	0.12	0.01	4	10
TC6	Air	Axisymmetric	Turbulent	0.245	422	0.10	0.10	4	10

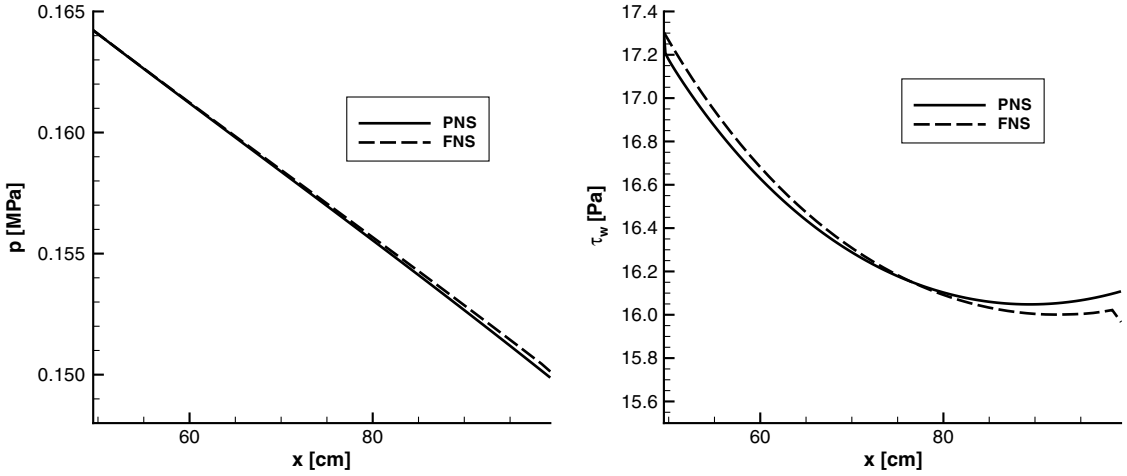

a) Pressure b) Wall shear stress

Fig. 3 Comparisons between FNS and PNS for a 2-D planar adiabatic laminar flow (TC1).

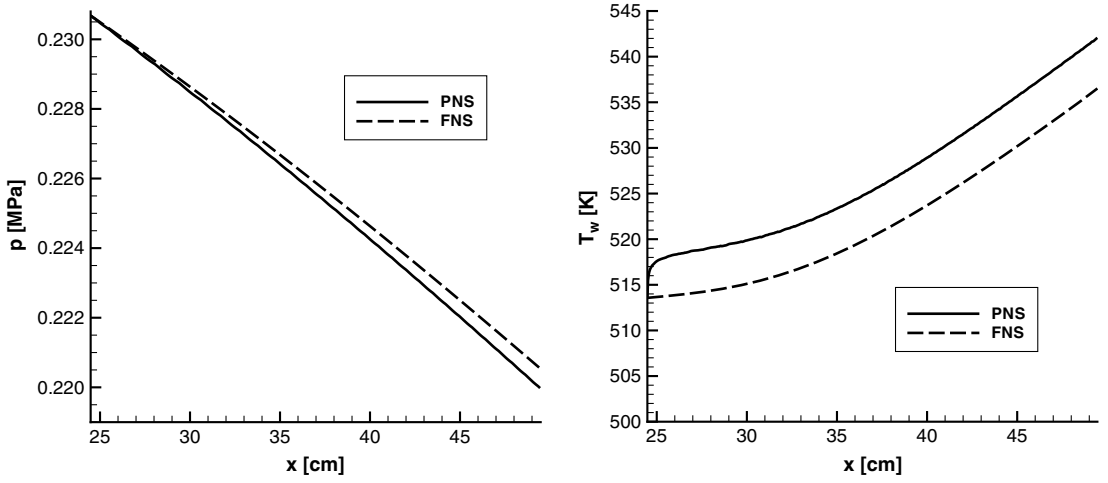

a) Pressure b) Wall shear stress

Fig. 4 Comparisons between FNS and PNS for a 2-D planar heated turbulent flow of air in perfect-gas conditions (TC2).

those studied in the foregoing section should be considered. To reach this goal, for a correct validation of the PNS solver, a test case has been selected for which experimental data are available in the open literature. In particular, the selected test case is one of those presented in [21], which is a detailed experimental study of hydrogen flow in heated tubes at sub- and supercritical pressures. Among all the test cases, 64_706 has been selected because of the particular thermodynamic condition of the hydrogen, which can be of great

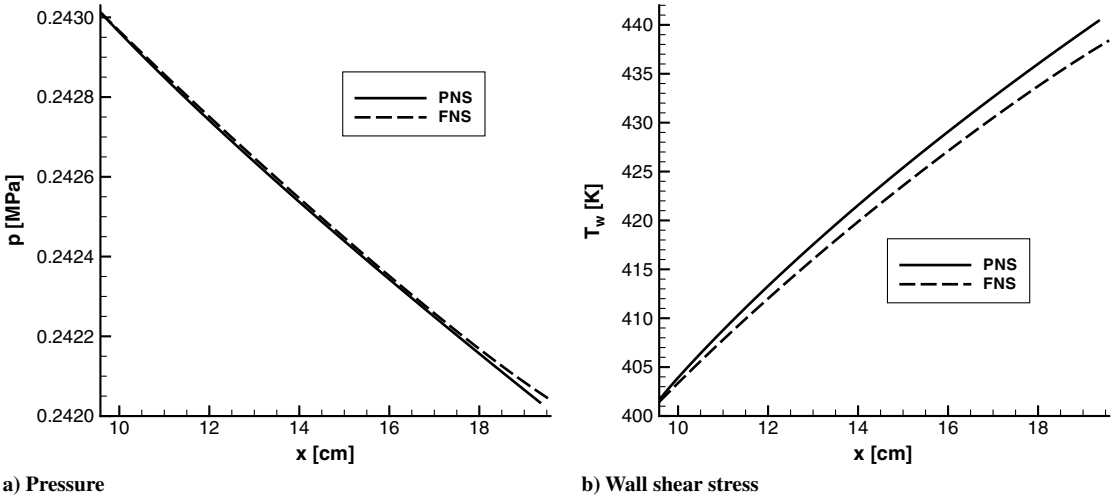

a) Pressure b) Wall shear stress

Fig. 5 Comparisons between FNS and PNS for a 2-D axisymmetric heated laminar flow of air in perfect-gas conditions (TC3).

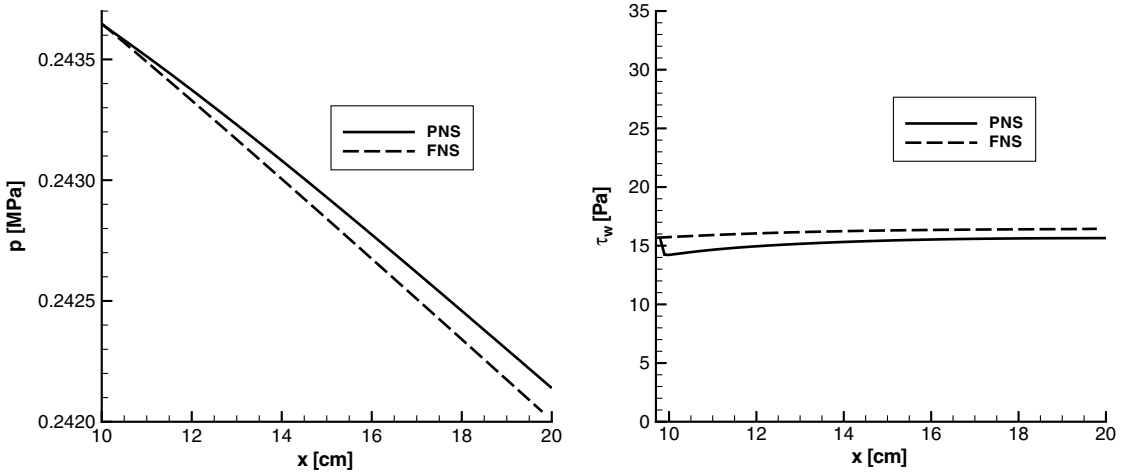

a) Pressure b) Wall shear stress

Fig. 6 Comparisons between FNS and PNS for a 2-D axisymmetric adiabatic turbulent flow of air in perfect-gas conditions (TC4).

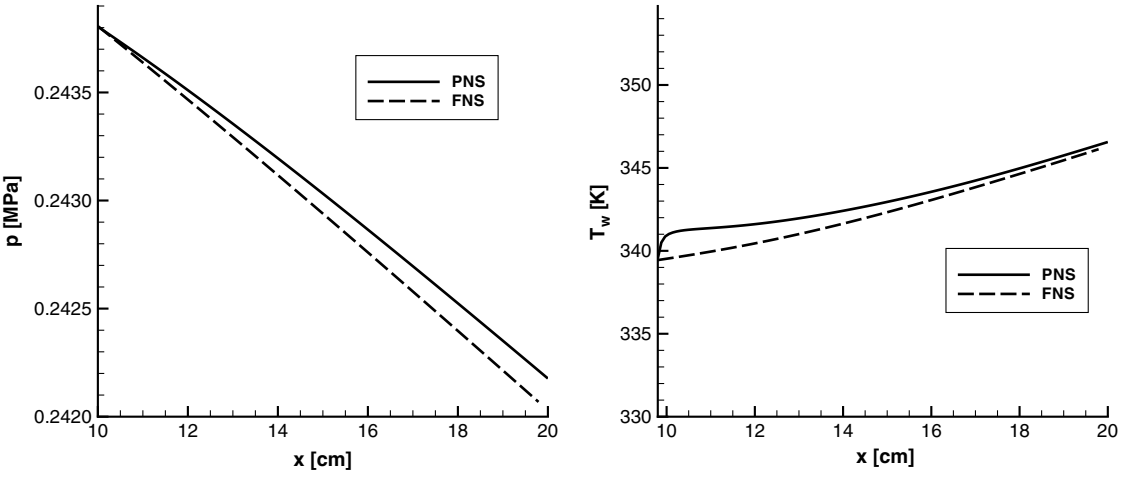

a) Pressure b) Wall shear stress

Fig. 7 Comparisons between FNS and PNS for a 2-D axisymmetric heated turbulent flow of air in perfect-gas conditions (TC5).

interest in the field of rocket cooling channels. Test-case inlet and exit temperature are 25 and 53 K, respectively, and the inlet pressure is 5 MPa. Consequently, hydrogen operative condition is transcritical; in fact, the pressure is supercritical ($p/p_c \simeq 3.8$), the inlet temperature is subcritical ($T/T_c \simeq 0.8$), and the exit temperature is supercritical ($T/T_c \simeq 1.8$).

This test case is of particular interest because it presents heat transfer deterioration. This phenomenon can appear in the case of

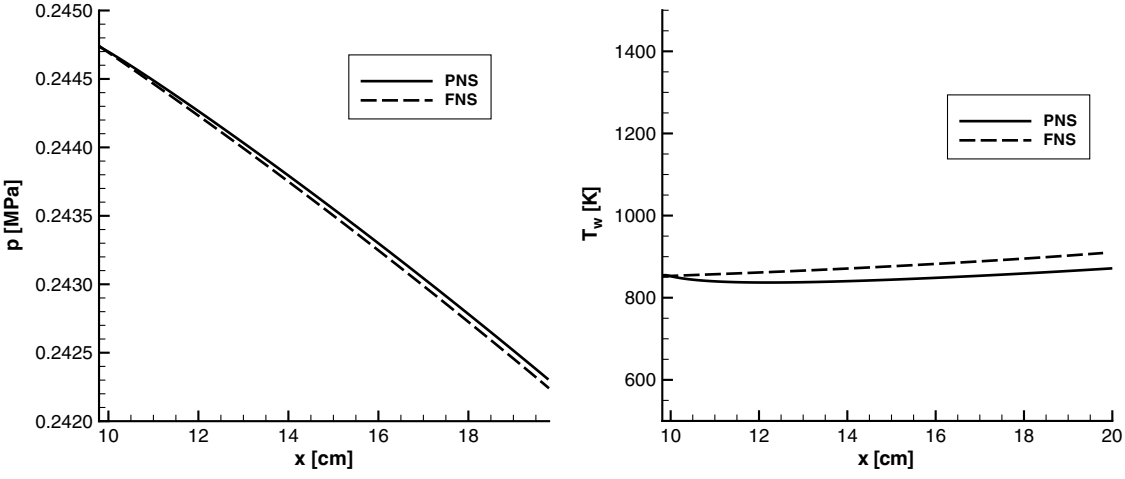

a) Pressure b) Wall shear stress

Fig. 8 Comparisons between FNS and PNS for a 2-D axisymmetric heated turbulent flow of air in perfect-gas conditions (TC6).

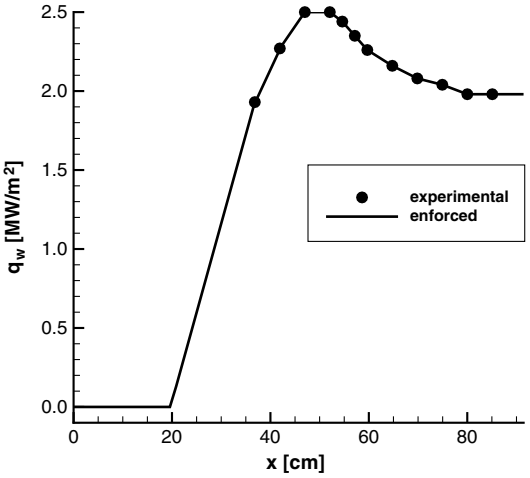

Fig. 9 Enforced and experimental heat flux.

supercritical-pressure fluids with pressure and temperature close to the critical ones (near-critical fluids). In fact, if such a fluid is heated up in a channel and passes from a temperature smaller than the pseudocritical temperature T_{ps} to a temperature greater than T_{ps}, a pseudo phase change occurs [27,28] (the pseudocritical temperature is the temperature at which specific heat at constant pressure has a maximum at a specified pressure). The fluid passes from a liquidlike to a gaslike state, with an abrupt change in all the properties [29]. This can lead to a deterioration of the heat transfer at low mass flow rate, high heat flux and fluid and wall temperatures being, respectively, lower and higher than the pseudocritical value [9,30–32]. In fact, due to the large heat flux, the temperature near the wall increases along the tube and exceeds the pseudocritical temperature. As a consequence, the density undergoes an abrupt fall; a gaseous film appears near the wall, characterized by a low thermal capacity and a low density. This causes a deterioration of the heat transfer and thus a great increase in the wall temperature. More downstream, the bulk temperature reaches the pseudocritical value, leading to an increase in the velocity and thus in the heat transfer; as a result, the wall temperature decreases. As a matter of fact, if the deterioration occurs, the wall temperature first grows and then decreases; that is, it shows a peak.

The mass flow rate per unit area of the tube cross section is 1324 kg/m^2 s. The experimental apparatus is composed by a straight tube that has a length of 91.44 cm and an internal diameter of 8.51 mm and is electrically heated (the nominal heat flux is 2.35 MW/m^2) in the last part of the tube, whereas the first one-third of the tube is unheated in order to have a developed flowfield in the heated region [21]. The experimental results are measured in the heated part of the tube by means of surface thermocouples, pressure taps, and voltage-measurement devices. Computations are made of the 2-D axisymmetric configuration, enforcing the following inlet boundary conditions inferred from experimental data: static pressure $p_{in} = 5.0012$ MPa, density $\rho_{in} = 71.65$ kg/m^2, velocity $u_{in} = 18.5045$ m/s, and $v_{in} = 0$ m/s. These conditions provide the same values as in the experimental test of static temperature and static pressure at the first instrumented test section and mass flow rate. Moreover, zero heat flux has been imposed in the first part of the tube and a nonconstant heat flux distribution has been imposed in the remaining length, as reported in [21]. In fact, the measured heat flux

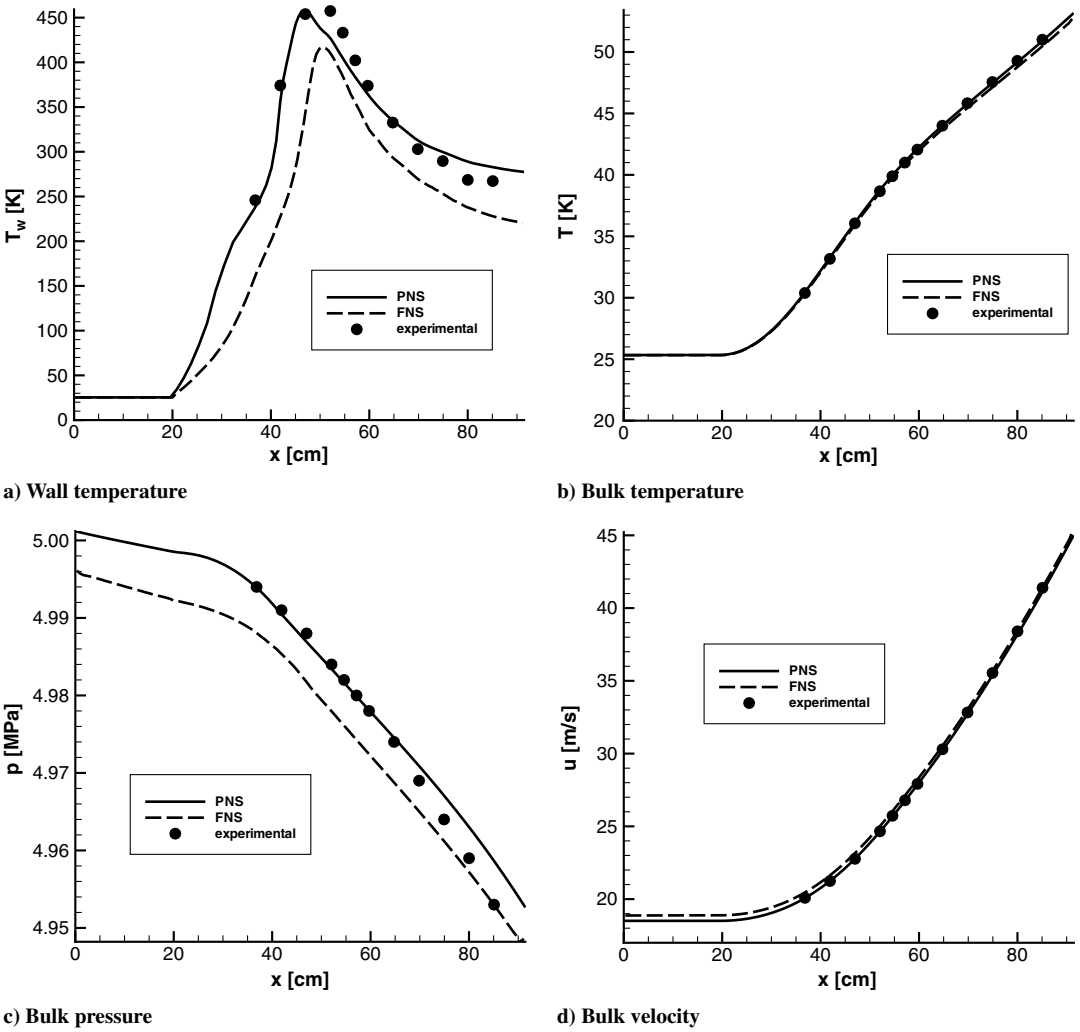

a) Wall temperature **b) Bulk temperature**

c) Bulk pressure **d) Bulk velocity**

Fig. 10 Comparisons between experimental data and numerical results.

is different from that theoretically enforced, because of the dependence of the channel material electric resistance on temperature and because of heat conduction through channel walls. For the latter reason, the heat flux is also nonzero in the nominal unheated region, and a linear interpolation has been assumed to enforce the smooth transition between the adiabatic and heated part of the channel (Fig. 9).

The numerical results are compared with the experimental data in Fig. 10 in terms of wall temperature and bulk temperature, pressure, and velocity. Note that the heat flux deterioration is shown by the large peak of wall temperature (see Fig. 10a) occurring at $x \simeq 50$ cm. As can be seen in Fig. 10b, the bulk temperature behavior is very well reproduced by the numerical simulation, with a discrepancy smaller than 0.2%. Computed bulk pressure (Fig. 10c), velocity (Fig. 10d), and density (not shown here) also fall in the range of experimental test results, as the maximum discrepancy is only 0.1% for pressure, 0.5% for the density, and 0.6% for the velocity. The wall temperature (Fig. 10a) shows a larger discrepancy, which remains smaller than 6%, however. These comparisons are very satisfactory. In fact, the data of [21] are affected by an estimated experimental error of 3% for the mass flow rate, 4% for the inlet fluid temperature, and 1% for the fluid pressure. Moreover, because the value of material electric resistance is considered to be no better than 10% accurate, the same uncertainty affects the estimate of the heat flux, as it is a function of the electric power supplied and the wall material resistance.

For the sake of completeness, the results presented in Fig. 10 are also compared with grid-converged FNS simulations carried out for this test case in [7]. As shown in the foregoing section, there are differences between PNS and FNS results. However, if compared with experimental data, both results are included within the data uncertainty. In particular, good agreement is found on the bulk properties, whereas there is a greater discrepancy in the evaluation of wall properties (for instance, see the wall temperature in Fig. 10a). It is interesting to note that in this case, PNS results are even closer to experimental data than are FNS results. Although the extremely high resolution in the streamwise direction of PNS and the different way of enforcing inlet and outlet boundary conditions could provide a partial explanation, the greater closeness of PNS results to experimental data with respect to FNS should be considered as fortuitous. The overall result, however, is that both approaches can be used to reasonably predict the flows of interest, as confirmed by comparison with experimental data. In addition, the most important result for the objectives of the present study is that the PNS approach also provides solutions close to FNS in the case of turbulent heated flow of a near-critical fluid.

The good agreement between experimental data and numerical results on this test case therefore proves that the PNS solver could be a suitable tool to study complex thermodynamic phenomena, such as heat transfer deterioration, which is a phenomenon likely to occur in liquid rocket engine cooling channels.

VII. Computational Time

The main advantage of the PNS approach with respect to the FNS consists of a considerable saving of computational time. A quantification of the saving has been carried out by comparing the time it takes to compute the same flowfield with the two approaches. The test case is the TC4 of Table 1, except for the length, which is $L = 20$ cm (that is, 50 diameters). The same mesh in the transverse direction has been adopted for both the computations. The end of the computation with the two codes is obviously established by different criteria; the FNS simulation is continued until iterative convergence to the steady state is achieved, and the PNS simulation finishes when the end of the tube is reached. The computations have been carried out on an Intel processor, Core2, quad core, with a 2.5 GHz CPU. The FNS computation took $\Delta t_{\text{FNS}} = 7895$ s, whereas the PNS computation only took $\Delta t_{\text{PNS}} = 299$ s: that is, more than 25 times less. This is an illustrative case, but the same order of computational-time saving was obtained in all configurations.

VIII. Conclusions

A first step toward the development of a parabolized Navier–Stokes equations solver to study the flow evolution in the cooling channels of a liquid-propellant rocket engine has been carried out. The main advantage of this approach consists of a substantial saving of computational time, which will allow more sophisticated phenomena modeling in the future than that allowed by the solution of the unsteady full Navier–Stokes equations. In the present study the two-dimensional and axisymmetric turbulent compressible flows have been considered in a generic thermodynamic state (perfect gas, real gas, near-critical fluid, etc.). Validation has been carried out by a comparison with numerical results obtained with a full Navier–Stokes equations solver for 2-D planar and 2-D axisymmetric flows on air in a perfect-gas condition. The results allow one to quantify how well the parabolized Navier–Stokes equations can describe the heated-channel-flow behavior. Finally, a further validation has been carried out by comparison with other numerical results and experimental data for a test case representative of liquid rocket engine cooling-channel flows. The comparison with experimental data has been carried out for a heated-channel turbulent flow of hydrogen in a near-critical condition, which exhibits heat transfer deterioration. The good agreement between the experimental data and the numerical results is a confirmation of the validity of the parabolized Navier–Stokes equations approach for the study of the channel flows of interest in liquid rocket engine design. In addition, it proves that the present parabolized Navier–Stokes equations solver is able to describe complex thermodynamic phenomena, such as heat transfer deterioration. These results give confidence in the future development of the present numerical tool.

References

[1] LeBail, F., and Popp, M., "Numerical Analysis of High Aspect Ratio Cooling Passage Flow and Heat Transfer," 29th AIAA/ASME/SAE/ASEE Joint Propulsion Conference, AIAA Paper 1993-1829, June 1993.

[2] Woschnak, A., and Oschwald, M., "Thermo and Fluidmechanical Analysis of High Aspect Ratio Cooling Channels," 37th AIAA/ASME/SAE/ASEE Joint Propulsion Conference, AIAA Paper 2001-3404, July 2001.

[3] Jung, H., Merkle, C., Schuff, R., and Anderson, W., "Detailed Flowfield Predictions of Heat Transfer to Supercritical Fluids in High Aspect Ratio Channels," 43rd AIAA/ASME/SAE/ASEE Joint Propulsion Conference, AIAA Paper 2007-5548, July 2007.

[4] Pizzarelli, M., Nasuti, F., and Onofri, M., "A Simplified Model for the Analysis of Thermal Stratification in Cooling Channels," *2nd European Conference for Aerospace Sciences*, von Karman Inst. for Fluid Dynamics, Brussels, July 2007.

[5] Pizzarelli, M., Nasuti, F., Paciorri, R., and Onofri, M., "Numerical Analysis of Three-Dimensional Flow of Supercritical Fluid in Cooling Channels," *AIAA Journal*, Vol. 47, No. 11, Nov. 2009, pp. 2534–2543.
doi:10.2514/1.38542.

[6] Knab, O., Frey, M., Grgen, J., Maeding, C., Quering, K., and Wiedmann, D., "Progress in Combustion and Heat Transfer Modelling in Rocket Thrust Chamber Applied Engineering," 45th AIAA/ASME/SAE/ASEE Joint Propulsion Conference, AIAA Paper 2009-5477, Aug. 2009.

[7] Pizzarelli, M., Urbano, A., and Nasuti, F., "Numerical Analysis of Deterioration in Heat Transfer to Near-Critical Rocket Propellants," *Numerical Heat Transfer, Part A, Applications*, Vol. 57, 2010, pp. 297–314.
doi:10.1080/10407780903583016

[8] Di Matteo, F., De Rosa, M., and Onofri, M., "Semi-Empirical Heat Transfer Correlations in Combustion Chambers for Transient System Modelling," *Space Propulsion Conference 2010*, Spain, May 2010.

[9] Wang, Y.-Z., Hua, Y.-X., and Meng, H., "Numerical Studies of Supercritical Turbulent Convective Heat Transfer of Cryogenic-Propellant Methane," *Journal of Thermophysics and Heat Transfer*, Vol. 24, No. 3, 2010, pp. 490–500.
doi:10.2514/1.46769

[10] Higashino, K., Sugioka, M., Kobayashi, T., Minato, R., and Maru, Y., "Fundamental Study on Coking Characteristics of LNG Rocket Engines," 44th AIAA/ASME/SAE/ASEE Joint Propulsion Conference, AIAA Paper 2008-4753, 2008.

[11] Woschnak, A., Suslov, D., and Oschwald, M., "Experimental and Numerical Investigation of Thermal Stratification Effects," 39th AIAA/ASME/SAE/ASEE Joint Propulsion Conference, AIAA Paper 2003-4615, July 2003.

[12] Rubin, S., and Tannehill, J., "Parabolized/Reduced Navier–Stokes Computational Techniques," *Annual Review of Fluid Mechanics*, Vol. 24, 1992, pp. 117–144.

[13] Wadawadigi, G., Tannehill, J., and Buelow, P., "Three-Dimensional Upwind Parabolized Navier–Stokes Code for Supersonic Combustion Flowfileds," *Journal of Thermophysics and Heat Transfer*, Vol. 7, No. 4, 1993, pp. 661–667.
doi:10.2514/3.475

[14] Buelow, J. C. P., Tannehill, J., Ievalts, J., and Lawrence, L., "Three-Dimensional, Upwind, Parabolized Navier–Stokes Code for Chemically Reacting Flows," *Journal of Thermophysics and Heat Transfer*, Vol. 5, No. 3, 1991, pp. 274–283.
doi:10.2514/3.261

[15] Briley, W., "Numerical Method for Predicting Three-Dimensional Steady Viscous Flow in Ducts," *Journal of Computational Physics*, Vol. 14, 1974, pp. 8–28.
doi:10.1016/0021-9991(74)90002-3

[16] Anderson, O., "Calculation of Internal Viscous Flows in Axisymmetric Ducts at Moderate to High Reynolds Numbers," *Computers and Fluids*, Vol. 8, 1980, pp. 391–411.
doi:10.1016/0045-7930(80)90002-X

[17] Govindan, T., and Lakshminarayana, B., "A Space-Marching Method for the Computation of Viscous Internal Flows," *Computers and Fluids*, Vol. 16, 1988, pp. 21–39.
doi:10.1016/0045-7930(88)90036-9

[18] Chilukuri, R., and Pletcher, R., "Numerical Solutions to the Partially Parabolized Navier–Stokes Equations for Developing Flow in a Channel," *Numerical Heat Transfer*, Vol. 3, 1980, pp. 169–188.
doi:10.1080/01495728008961753

[19] Murthy, J., and Patankar, S., "A Partially Parabolic Calculation Procedure for Duct Flows in Irregular Geometries. Part I: Formulation," *Numerical Heat Transfer, Part B, Fundamentals*, Vol. 16, 1989, pp. 1–15.
doi:10.1080/10407798908944925

[20] Tannehill, J., Anderson, D., and Pletcher, R. H., *Computational Fluid Mechanics and Heat Transfer*, Taylor & Francis, New York, 1984.

[21] Hendricks, R., Graham, R., Hsu, Y., and Friedman, R., "Experimental Heat-Transfer Results for Cryogenic Hydrogen Flowing in Tubes at Subcritical and Supercritical Pressures to 800 Pounds per Square Inch Absolute," NASA TN D-3095, 1966.

[22] Vigneron, Y., Rakich, J., and Tannehill, J., "Calculation of Supersonic Viscous Flow over Delta Wings with Sharp Subsonic Leading Edges," AIAA Paper 78-1137, 1978.

[23] Spalart, P., and Allmaras, S., "A One-Equation Turbulence Model for Aerodynamic Flow," *La Recherche Aerospatiale*, Vol. 1, 1994, pp. 5–21.

[24] Roe, P., "Approximate Riemann Solvers, Parameter Vectors, and Difference Schemes," *Journal of Computational Physics*, Vol. 43, 1981, pp. 357–372.
doi:10.1016/0021-9991(81)90128-5

[25] Younglove, B., "Thermophysical Properties of Fluids. I. Argon, Ethylene, Parahydrogen, Nitrogen, Nitrogen Trifluoride, and Oxygen," *Journal of Physical and Chemical Reference Data*, Vol. 11, No. 1, 1982, pp. 1–77.
doi:10.1063/1.555661

[26] Younglove, B., and Ely, J., "Thermophysical Properties of Fluids. II. Methane, Ethane, Propane, Isobutane, and Normal Butane," *Journal of Physical and Chemical Reference Data*, Vol. 16, No. 4, 1987, pp. 577–798.

[27] Sato, T., Sugiyama, M., Itoh, K., Mori, K., Fukunaga, T., Misawa, M., Otomo, T., and Takata, S., "Structural Difference Between Liquidlike and Gaslike Phases in Supercritical Fluid," *Physical Review E (Statistical, Nonlinear, and Soft Matter Physics)* Vol. 78, No. 5, 2008, Paper 051503.
doi:10.1103/PhysRevE.78.051503

[28] Zhong, F., Fan, X., Yu, G., Li, J., and Sung, C., "Heat Transfer of Aviation Kerosene at Supercritical Conditions," *Journal of Thermophysics and Heat Transfer*, Vol. 23, No. 3, 2009, pp. 543–550.
doi:10.2514/1.41619

[29] Koshizuka, S., Takano, N., and Oka, Y., "Numerical Analysis of Deterioration Phenomena in Heat Transfer to Supercritical Water," *International Journal of Heat and Mass Transfer*, Vol. 38, No. 16, 1995, pp. 3077–2084.
doi:10.1016/0017-9310(95)00008-W

[30] Cheng, X., Kuang, B., and Yang, Y., "Numerical Analysis of Heat Transfer in Supercritical Water-Cooled Flow Channels," *Nuclear Engineering and Design*, Vol. 237, No. 3, 2007, pp. 240–252.
doi:10.1016/j.nucengdes.2006.06.011

[31] Shiralkar, B., and Griffith, P., "Deterioration in Heat Transfer to Fluids at Supercritical Pressure and High Heat Fluxes," *Journal of Heat Transfer*, Vol. 91, No. 1, Feb. 1969, pp. 27–36.

[32] Graham, R. W., Hendricks, R. C., and Simoneau, R. J., "Convective Heat Transfer to Low-Temperature Fluids," *Heat Transfer at Low Temperatures*, Plenum, New York, 1974.